Energy & Buildings 338 (2025) 115672

Contents lists available at ScienceDirect

Energy & Buildings

journal homepage: www.elsevier.com/locate/enb

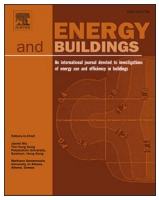

# Enhancing ventilated roof performance: A study on Maisotsenko indirect evaporative cooling for school buildings☆

Nicolò Morselli, Marco Puglia, Michele Cossu, Simone Pedrazzi, Giulio Allesina, Paolo Tartarini, Alberto Muscio *

*Dipartimento di ingegneria "Enzo Ferrari", Università degli Studi di Modena e Reggio Emilia, Via Vivarelli 10/1, 41125 Modena, Italy*

A B S T R A C T

A ventilated roof consists of generating a series of ducts inside the roof of a building through the creation of openings near the rain gutters and on the ridge. Although in pitched roofs airflow is often buoyancy driven, for horizontal roofs or to enhance performance, forced convection becomes necessary. This study explores the use of a commercially available M-cycle evaporative cooler as a multifunctional solution for thermal management and ventilation in school buildings. By integrating the M-cycle with a ventilated roof, the study focuses on optimizing air renewal and cooling through the use of product air, while the working air, typically wasted, is used to ventilate the roof cavity. By employing an approach that combines psychrometric, analytical, and *CFD* models, it is demonstrated that, on a traditional roof configuration with cavity on top, the M-cycle can reduce solar gain by up to 68% when working air is used to ventilate the cavity. Furthermore, it is shown that the positioning of the ventilated cavity plays a crucial role, providing the best results when facing indoors. In such cases, it contributes to a solar gain reduction of up to 94%, leading to the development of a radiant cold surface that actively assists in cooling the room. These findings provide a first insight on a sustainable solution that can be applied beyond the specific case study, improving indoor climate control and reducing environmental impact.

## 1. Introduction

Most daily activities now take place indoors, making the building sector the largest global energy consumer [1], with significant impacts on resource consumption and climate change. In the United States, for instance, electricity consumption has increased significantly, rising from approximately 281 billion kWh in 1950 to 4.07 trillion kWh in 2022, a fourteen-fold increase. This growth reflects the increasing reliance on electricity for lighting, heating, cooling, and other essential applications. Among these, space cooling is a major contributor, accounting for 16.2 % of residential electricity consumption in 2022, highlighting its significant role in total energy use [2].

This scenario underscores the urgency of finding solutions to improve energy efficiency by reducing consumption and maximizing resource utilization. The issue becomes critical in indoor space design, where architectural choices affect not only energy use but also the comfort and health of occupants. Air quality directly impacts physical well-being, while lighting and acoustics play key roles in the overall perception of space [3] and exposure to indoor pollutants can cause health problems, including asthma, allergies, and even severe diseases like lung cancer [4]. Phenomena such as Sick Building Syndrome (SBS), which include symptoms like eye irritation, headaches, and respiratory difficulties, are frequently reported in workplaces or study environments [5]. Such conditions are often associated to inadequate ventilation, high $CO_2$ concentrations and the presence of volatile organic compounds (VOCs), formaldehyde, dust and other bioaerosol contaminants [6]. Indoor air quality (IAQ) and ventilation are also crucial for productivity in workplaces and learning capacity in educational buildings [7], with studies establishing correlations between student performance and environmental parameters such as air temperature, relative humidity, and $CO_2$ concentration [8].

However, analyses of ventilation rates in many schools, offices, and residential buildings have shown that recommended levels are often not achieved [9], with $CO_2$ concentrations frequently exceeding 1000 ppm and peaking at 6000 ppm in some cases [10]. Such high values are associated with worsening respiratory symptoms and reduced cognitive ability, whereas good air quality can significantly enhance productivity and learning. For instance, in educational settings, increased air renewal in classrooms has been linked to improvements in students' performance [10], further highlighting the importance of this aspect.

In building design, balancing energy efficiency, thermal comfort, and indoor air quality represents a complex challenge, referred to as the EE-TC-IAQ dilemma (energy efficiency, thermal comfort, indoor air quality) and densely occupied spaces, such as classrooms, require significant air exchange to maintain good air quality. However, this can increase

☆ This article is part of a special issue entitled: 'Sustainable energy communities' published in Energy & Buildings.

* Corresponding author.
*E-mail address:* alberto.muscio@unimore.it (A. Muscio).

https://doi.org/10.1016/j.enbuild.2025.115672
Received 23 November 2024; Received in revised form 10 February 2025; Accepted 26 March 2025
Available online 30 March 2025
0378-7788/© 2025 The Author(s). Published by Elsevier B.V. This is an open access article under the CC BY license (http://creativecommons.org/licenses/by/4.0/).

**Nomenclature**

*Parameters*

| | |
|---|---|
| $c$ | $\frac{J}{kgK}$, Specific heat capacity |
| $CC$ | $W$, Cooling capacity |
| $c_p$ | $\frac{J}{kgK}$, Specific heat capacity at constant pressure |
| $h$ | $\frac{W}{m^2K}$, Convective heat transfer coefficient |
| $h_{lv}$ | $\frac{J}{kg}$, Latent heat of vaporization |
| $\dot{m}$ | $\frac{kg}{s}$, Mass flow rate |
| $M$ | $\frac{g}{mol}$, Molar mass |
| $n$ | $mol$, Number of moles |
| $p$ | $Pa$, Pressure |
| $R$ | $\frac{J}{kmolK}$, Universal gas constant |
| $r_V$ | $-$, Supply to inlet volume flow ratio |
| $r_m$ | $-$, Supply to inlet mass flow ratio |
| $T$ | $K$, Temperature |
| $\dot{V}$ | $\frac{m^3}{s}$, Volume flow rate |

*Greek letters*

| | |
|---|---|
| $\alpha$ | $-$, Absorption coefficient |
| $\in$ | $-$, Thermal emissivity |
| $\lambda$ | $\frac{W}{mK}$, Thermal conductivity |
| $\rho$ | $\frac{kg}{m^3}$, Density |
| $\varphi$ | $-$, Relative humidity |

*Subscripts*

| | |
|---|---|
| *amb* | External Environment |
| *channel* | Referred to 7.2x1 $m^2$ bottom surface of the ventilated channel |
| *ceiling* | Referred to 6.8*7.2 $m^2$ internal surface of each classroom ceiling |
| *da* | Dry air mixture |
| *di* | Dry channel inlet |
| *do* | Dry channel outlet |
| *DB* | Dry bulb temperature |
| *gyp* | Drywall |
| *h* | Referred to convection |
| *k* | Referred to conduction |
| *l* | Liquid state |
| *m* | Metal |
| *met* | Metabolic |
| *p* | Product air |
| *room* | Internal environment |
| *s* | Surface |
| *sat* | Vapor saturation condition |
| *v* | Vapor state |
| *WB* | Wet bulb temperature |
| *wo* | Wet channel outlet |
| *wood* | Wooden decking |
| *XPS* | Insulating foam |

energy consumption for heating or cooling. Solutions such as summer night-time free ventilation, optimizing building envelope insulation, and managing solar gains can reduce energy costs while maintaining high comfort standards [11]. Moreover, climate-specific and site-specific building design is essential, i.e, in cold climates, enhancing thermal insulation can significantly reduce energy consumption, while in hot climates, reducing solar gains and improving cooling system efficiency becomes a priority.

The choice of HVAC (Heating, Ventilation, and Air Conditioning) systems also plays a crucial role in this balance and evaporative cooling cycles offer an energy-efficient alternative to traditional vapor compression refrigerators (VCR). These systems have evolved significantly, from direct evaporative architectures, which are simple in design but problematic due to increased absolute air humidity, to the Maisotsenko cycle (M-cycle), which has introduced a revolutionary change in evaporative cooling systems [12].

The M-cycle uses the same concept of dry and wet channels of indirect evaporative coolers but modifies the airflow path to create a new thermodynamic cycle capable of moving the lower temperature limit from the wet bulb to the dew point temperature of the incoming air. This is achieved by diverting a portion of the total airflow entering the dry channel, into the wet channel (*working air*), where the latent heat of evaporation removes heat from the dry side through a heat transfer surface that separates the two ducts. Due to the slope of the saturation curve, a small increase in *working air* humidity results in a significant temperature drop in the *product air* [13], which refers to the portion of air that is not directed into the wet channel but rather delivered to the indoor environment to be cooled. At the end of the process, the working air, nearly saturated, is typically exhausted to the external environment.

M-cycle systems, extensively studied in the literature, both experimentally and numerically, have demonstrated potential in cross-flow and counter-flow configurations, each offering distinct advantages. Experimental investigations on M-cycle heat exchangers in counter-flow configurations have demonstrated their high cooling capacity, making them particularly suitable for applications requiring efficient heat dissipation. Under typical HVAC operating conditions, their Energy Efficiency Ratio (EER) values range from 2.8 to 15.5 [14], with energy savings of up to 58.7 % (compared to VCR) reported for the cooling demand in certain cities in China [15].

Despite their promising advantages, evaporative coolers are highly dependent on environmental conditions and often cannot achieve the same cooling capacity as VCR systems. Additionally, they require a continuous supply of fresh air to sustain the evaporation process and dissipate latent heat and, as a result, buildings equipped with evaporative coolers must maintain constant air exchange, which can lead to excessively high air velocities due to the large volumetric airflow rates involved. However, this characteristic can also be exploited as an effective solution to ensure proper ventilation in enclosed spaces while simultaneously removing internal heat.

The M-cycle is therefore more easily integrated into VCR systems rather than serving as a standalone solution for cooling buildings such as schools, offices, and similar non-industrial spaces, where an indoor setpoint temperature is often required regardless of external climate conditions. In this context, the M-cycle can help to reduce energy usage by pre-cooling the airflow supplied indoors, fulfilling the need for air exchange while lowering the energy demand of the VCR system [16].

A further strategy to improve building's energy efficiency, during hot seasons, is the adoption of a ventilated roof. Consisting of two layers separated by an air gap that acts as a ventilation channel, a ventilated roof reduces heat transfer indoors, thus limiting cooling energy demand [17]. The ventilated cavity is located between the top layer of tiles, which usually sits on a waterproofing membrane and a supporting slab, and the underlying roof structure. Air enters through vents near the gutters, moves upward through the cavity following the roof slope, and exits through ridge openings. This continuous airflow naturally removes the heat absorbed from solar radiation and under high solar irradiance, ventilated roofs demonstrate significant reductions in heat flux transferred indoors compared to non-ventilated roofs [18].

Their performance also relies on the stratigraphy and placement of the insulation layer, which should be located between the ceiling and the ventilation channel for the best results in roofs ventilated with external ambient air [19]. The choice of roof covering is also crucial to

avoid extreme surface temperatures caused by solar radiation and the most common option are clay tiles. Nevertheless corrugated sheet metal roofs (which function as a radiative barrier when properly coated) are gaining popularity due to their durability and lightweight properties, providing an alternative approach for energy-efficient building design [20].

The functioning of a ventilated roof, as described, is limited to pitched roofs, where natural airflow is driven by temperature and density gradients within the ventilated cavity. In this context, various studies have explored ways to enhance natural ventilation thorough examination of different influencing factors, including roof length, external atmospheric pressure, the integration of phase change materials [21], incorporating radiant barriers within the cavity [22] and implementing thermal breakers to reduce heat conduction through structural elements [23]. However, natural airflow in real applications is often weak and inconsistent, and its effectiveness can be further compromised when high ambient temperatures result in the intake of excessively warm air into the roof cavity. To address these limitations, forced ventilation strategies have been investigated to both stabilize and regulate airflow based on environmental conditions and to extend the benefits of ventilated roofs to flat surfaces [24].

Alongside these strategies, evaporative cooling stands out as a potential integration into roofs to reduce solar gains. In this regard, several studies explored a range of application technologies, including systems based on shaded water ponds [25] or spray cooling [26], as well as solutions employing porous materials, such as tiles or specialized layers, to promote evaporation. Integrated water ponds in roofs, for example, have proven effective in reducing heat in both tropical climates [27] and arid ones [28], even if they pose the problem of roof waterproofing, inefficient water use, and the risk of bacterial proliferation. On the other hand, configurations that use porous tiles [29] or hydrophilic material layers [30] can effectively lower roof surface temperatures while optimizing water consumption.

An alternative approach involves the use of evaporative coolers to saturate the air before it is introduced into a ventilated roof cavity, as studied by Pedrazzi et al. [31]. This technique not only maximizes the cooling potential of evaporated water but also prevents condensation within the cavity. By eliminating the structural and maintenance complexities of systems with exposed water surfaces, this solution has proven to be an efficient and feasible alternative to evaporative cooling methods available in literature.

This study aims to advance the current state of the art, where evaporative coolers are used in ventilated roofs, by investigating the application of a commercially available M-cycle cooling system as a multifunctional solution for both thermal management and ventilation.

As previously mentioned, this indirect evaporative cooler generates a significant flow of waste air (working air), which, despite being much cooler than the ambient air, is saturated and therefore unsuitable for direct indoor cooling. The key novelty of this approach lies in utilizing the *working air* to ventilate a flat roof while simultaneously using the *product air* to ensure indoor air renewal, contributing to cooling.

To minimize the variables involved, this solution was tested using an ideal school building as a case study, allowing the definition of specific occupancy levels, room dimensions and air exchange rates and providing a preliminary tool for evaluating the feasibility of this solution also as a retrofit option for existing buildings.

This represents an initial attempt at an integrated approach that optimizes both the building envelope and the HVAC system, going beyond conventional methods in the literature, which typically treat the building structure and HVAC systems as separate entities.

The aim is to produce findings that extend beyond the specific case study and can be applied to broader contexts.

In this work, the M-cycle is considered integrated with a vapor compression refrigeration (VCR) system designed to maintain the indoor spaces' dry-bulb temperature at a predetermined level. Different roof stratigraphies will be analysed to determine the optimal positioning of both the ventilated cavity and the insulation layer under various climatic conditions. Additionally, different ventilation strategies will be explored based on the external and working air temperatures.

The next chapter presents the initial case study, which is crucial for identifying the problem and narrowing the focus to key variables. This is followed by a description of the analytical model that outlines the M-cycle's operation, providing the boundary conditions for the *CFD* analysis of heat transfer within the cavity and enabling the evaluation of the ventilated channel's performance.

## 2. Material and methods

### 2.1. Description of the case study

The case study examines the application of an evaporative cooling unit based on the M-cycle architecture to the ventilated and flat roof of a school building. This context allows the exploration of various strategies, which will be detailed later, for combining and utilizing different air sources for channel ventilation. Additionally, given the strong dependency of M-cycle performance on the specific machine selection, the analysis is focused on a case study featuring well-defined geometries that serves as a basis for generalizing the results.

This study does not aim to calculate the overall energy behaviour of the building, instead, the focus is on identifying a few application solutions for forced roof ventilation and evaluating their contributions, assuming that the performance of the rest of the structure remains unchanged while varying the roof configurations under investigation.

The widespread use of wooden roofs in the market is largely due to their ecological benefits and excellent seismic resistance and, for this reason, a timber roof with a thickness of 2.5 cm and a thermal conductivity of 0.12 W/(m K) was chosen for this study. For instance, this configuration is commonly used in Italy for newly built schools (particularly in areas undergoing post-seismic reconstruction) as recommended by the guidelines of the Ministry of Education [32]. These roofs are typically covered with an insulating layer and, depending on landscape constraints, finished with either metal sheets or tiles.

Some of these buildings already include ventilated roofs with an air cavity above the insulation layer, while, in other cases, natural ventilation was not considered due to the low or absent roof slope. In these situations, it can be investigated the possibility of retrofitting a horizontal forced ventilation channel above the existing roof. However, altering the external roof may not always be possible due to the presence of thermal, photovoltaic or HVAC systems and, as a result, the potential of installing a ventilation channel beneath the wooden decking can be explored too.

Usually, school classrooms have a floor area ranging from about 40 up to 70 square meters.

[33] and the building portion considered for sizing the cooling unit consists of three classrooms, each measuring 6.8 x 7.2 m, adjacent to one another and forming part of a larger block of classrooms that extends beyond these three.

The ventilated cavity has a thickness $d_c = 10cm$ (assuming the maximum thickness recommended by the UNI 9460:2008 [34]) and it extends along the entire length of the classroom (7.2 m) and across the entire width: a series of parallel channels of homogeneous dimensions are hypothesized.

Two different positionings of the cavity with respect to the insulating layer are considered: *cavity on top* and *cavity at bottom*.

Considering the case of creating a ventilation channel above an existing roof (this configuration will be referred to as *cavity on top*), the following stratigraphy is chosen and listed starting from the side closest to the interior: a 2.5 cm thick wooden decking ($\lambda_{wood} = 0.1\frac{W}{mK}$), an insulating foam layer ($\lambda_{XPS} = 0.03\frac{W}{mK}$) with variable thickness ($d_{XPS} = 5\$15cm$ to simulate different thermal transmittances and thermal conductivity in accordance with the minimum requirements based

on the climatic zone), the ventilated channel ($d_c = 10cm$) and an external covering made of painted sheet metal (thickness 0.1 cm and $\lambda_m = 52\frac{W}{mK}$) properly coated to reach an absorption coefficient $\alpha = 0.5$ and thermal emissivity $\epsilon = 0.9$.

When the channel is placed inside the building, e.g. as a suspended ventilation ceiling (this configuration will be referred to as *cavity at bottom*), the following stratigraphy from inside out is considered: drywall with thermal conductivity of $\lambda_{gyp} = 1\frac{W}{mK}$ and $d_{gyp} = 1.2cm$, the ventilation channel, wooden decking (2.5 cm), and insulating material faced to the external environment covered with the same metal sheet. Insulation is tested at different thicknesses also in this configuration.

Solar irradiance has been considered constant with a value equal to the hourly average from 8:00 AM to 2:00 PM (typical school operating hours), assuming a sunny day in July, when the school term has ended but the schools are often fully operational with summer camps and allows us to consider a worst-case scenario in terms of cooling demand. The daily variation of solar irradiance measured in the city of Modena (urban area) on 10 July 2023 is shown in the graph of Fig. 1 with the considered period highlighted, whose average is 780 W/m$^2$. This value was used for the incident radiation in each case.

Each classroom is considered to be maintained at a constant and uniform internal temperature $T_{room} = 27^{\circ}C$ (upper limit recommended by Legislative Decree 81/08), assuming the presence of a VCR system for summer cooling. The air change per hour is calculated following the UNI 10339:1995 standard, suggesting a rate up to $AC = 7\frac{L}{sperson}$ for a secondary high school, implemented as a worst case. The same standard also suggests a maximum occupancy rate $OR = 0.45\frac{person}{m^2}$, leading to a presence of 22 people per classroom. The people metabolic heat rate was considered constant at $\dot{Q}_{met} = 126\frac{W}{person}$ as suggested by the ISO 8996:2021 [35] and used in similar studies on air conditioning in school buildings [36].

The operation of evaporative coolers does not involve internal air recirculation sections, as there is no condensation stage like in VCRs.

The performance of the following operational configurations of the ventilated package are then considered:

- Ventilation with working or exhaust air: for this configuration, both *cavity on top* and *cavity at bottom* solutions are ventilated with working air when its temperature is lower than the room setpoint temperature. When the M-cycle operates with a working air outlet temperature above 27 °C, exhaust air exiting the room is used instead. Exhaust air is assumed to be expelled from the room at the room setpoint temperature.
- Ventilation with external air: in the absence of an M-cycle evaporative cooler and without altering the air extraction ducts, the configuration considered involves ventilating the *cavity on top* with air at ambient temperature, thereby simulating the behaviour of a traditional ventilated roof, even if with forced convection. This case is used as a baseline to measure the benefits of using exhaust air or working air.

A diagram of the different cavity positioning configurations and type of air used for ventilation is shown in Fig. 2.

For each scenario, in addition to varying the insulation thickness, five distinct climatic conditions were analysed to account for different outdoor air dry and wet-bulb temperatures while maintaining the same solar irradiance. These conditions correspond to those used by the manufacturer (Seeley International Inc.), whose data were used in the study:

- Arid ($T_{db} = 42^{\circ}C$, $T_{wb} = 21^{\circ}C$)
- Temperate ($T_{db} = 37^{\circ}C$, $T_{wb} = 19^{\circ}C$)
- Continental ($T_{db} = 31^{\circ}C$, $T_{wb} = 20^{\circ}C$)
- Sub-tropical ($T_{db} = 31^{\circ}C$, $T_{wb} = 23^{\circ}C$)
- Tropical ($T_{db} = 33^{\circ}C$, $T_{wb} = 26^{\circ}C$)

Each of these climates leads to different operating conditions of the evaporative cooler, generating variations in the temperatures of both the product air and the working air.

The following section describes in detail the operation of the identified evaporative cooler and presents the method for calculating the air temperatures at the cavity outlet under different environmental conditions.

### 2.2. M-cycle evaporative cooler

For the performance assessment of the M-cycle, the technical information were provided by Seeley International for the commercially available CW-H15 heat and mass exchanger model. A product air outlet

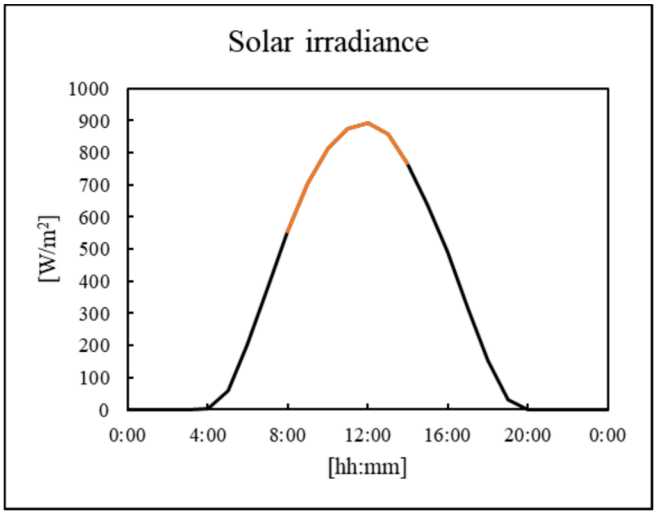


**Fig. 1.** Solar radiation trend measured on July 10, 2023, at latitude 44.6583 and longitude 10.9187 (ARPAE – Emilia Romagna Region Dext3r Database – https://simc.arpae.it/dext3r/).

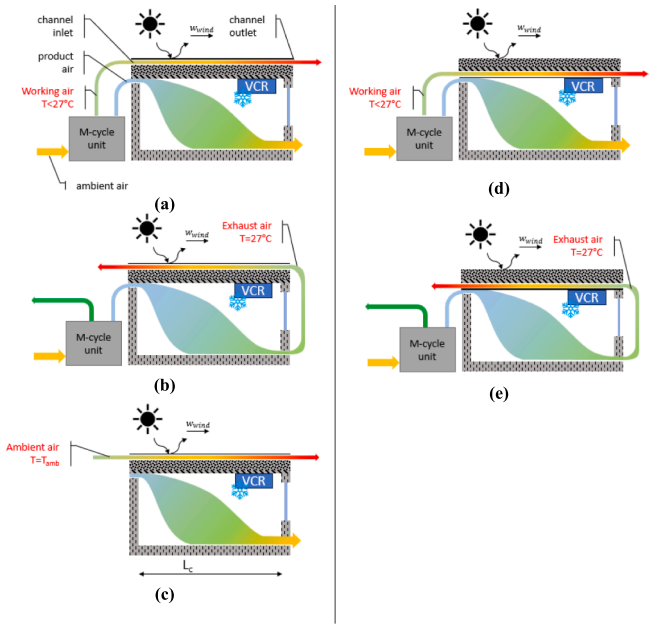


**Fig. 2.** Representation of the different analysed cases: cavity on top ventilated with working air (a), exhaust air (b) ambient air (c) and cavity at bottom configurations ventilated with working air (d) and exhaust air (e).

temperature ($T_p$) is provided according to the variation of the psychrometric conditions of the processed ambient air. The data regarding the outlet conditions of the air from the wet channel are not directly available; therefore, a calculation is necessary to estimate these parameters. According to Seeley International, the volumetric flow rate of the product air is considered constant at $3546 m^3/h$ and the product-to-inlet volumetric flow ratio is assumed to be constant and equal to 55 %:

$$r_V = \frac{\dot{V}_p}{\dot{V}_{di}} = 0.55 \tag{2.1}$$

For the conversion to the product-to-inlet mass flow ratio, the following relationship is applied:

$$r_m = \frac{\dot{m}_p}{\dot{m}_{di}} = \frac{\rho_p \dot{V}_p}{\rho_{di} \dot{V}_{di}} = \frac{\rho_p}{\rho_{di}} r_V \tag{2.2}$$

Knowing the inlet volumetric flow rate and thermo-hygrometric conditions $\dot{V}_{di}$, $T_{di}$, $\varphi_{di}$, $p_{di}$, it is possible to calculate the mass flow rates of water vapor $\dot{m}_{v,di}$, dry air $\dot{m}_{da,di}$, and therefore the total mass flow rate within the dry channel $\dot{m}_{di}$

$$\dot{m}_{v,di} = \frac{p_{v,di} \dot{V}_{di} M_v}{R T_{di}} = \frac{\varphi_{di} p_{v,sat,di}(T_{di}) \dot{V}_{di} M_v}{R T_{di}} \tag{2.3}$$

$$\dot{m}_{da,di} = \frac{p_{da,di} \dot{V}_{di} M_{da}}{R T_{di}} = \frac{(p_{di} - p_{v,di}) \dot{V}_{di} M_{da}}{R T_{di}} \tag{2.4}$$

$$\dot{m}_{di} = \dot{m}_{da,di} + \dot{m}_{v,di} \tag{2.5}$$

This value can be used to calculate the density of the humid air mixture at the inlet $\rho_{di}$ through the definition

$$\rho_{di} = \frac{\dot{m}_{di}}{\dot{V}_{di}} \tag{2.6}$$

The mass flow rate inside the dry channel remains constant along its entire length

$$\dot{m}_{do} = \dot{m}_{di} \tag{2.7}$$

From this, it is possible to calculate the volumetric flow rates at the outlet of the dry channel for dry air $\dot{V}_{da,do}$, water vapor $\dot{V}_{v,do}$, and consequently, the total volumetric flow rate at the outlet $\dot{V}_{do}$

$$\dot{V}_{da,do} = \frac{\dot{m}_{da,do} R T_{do}}{p_{do} M_{da}} \tag{2.8}$$

$$\dot{V}_{v,do} = \frac{\dot{m}_{v,do} R T_{do}}{p_{do} M_v} \tag{2.9}$$

$$\dot{V}_{do} = \dot{V}_{da,do} + \dot{V}_{v,do} \tag{2.10}$$

It is now possible to calculate the density of the humid air mixture at the outlet of the dry channel $\rho_{do}$, which can be assumed to be equal to the density of the product air $\rho_p$

$$\rho_{do} = \frac{\dot{m}_{do}}{\dot{V}_{do}} = \rho_p \tag{2.11}$$

At this point, the product to inlet mass flow ratio can be calculated through equation (2.2). The resulting mass flows at various locations can then be used in the overall mass and energy balance of the system. Considering the diagram in Fig. 3, the overall mass and energy balances for this heat exchanger is then formulated.

The mass balance of the dry gas mixture, considering the calculated mass flow ratio under the assumption of perfect mixing, is expressed as

$$\dot{m}_{da,di} = \dot{m}_{da,p} + \dot{m}_{da,wo} = r_m \dot{m}_{da,di} + \dot{m}_{da,wo} \tag{2.12}$$

leading to the relationship

$$\dot{m}_{da,wo} = \dot{m}_{da,di} - r_m \dot{m}_{da,di} = (1 - r_m) \dot{m}_{da,di} \tag{2.13}$$

The mass balance for water is written as

$$\dot{m}_{v,di} + \dot{m}_l = \dot{m}_{v,p} + \dot{m}_{v,wo} = r_m \dot{m}_{v,di} + \dot{m}_{v,wo} \tag{2.14}$$

from which the water consumption of the system can be calculated as

$$\dot{m}_l = (r_m - 1) \dot{m}_{v,di} + \dot{m}_{v,wo} \tag{2.15}$$

However, to calculate the water consumed, it is necessary to know the humidity at the outlet of the wet air stream. If this data is unavailable, an assumption must be made. By specifying the relative humidity at the outlet of the wet channel $\varphi_{wo}$, the relationship for the absolute humidity under this condition can be written.

$$\omega_{wo} = \frac{\dot{m}_{v,wo}}{\dot{m}_{da,wo}} = \frac{M_v}{M_{da}} \frac{p_{v,wo}}{p_{wo} - p_{v,wo}} = \frac{M_v}{M_{da}} \frac{\varphi_{wo} p_{v,sat}(T_{wo})}{p_{wo} - \varphi_{wo} p_{v,sat}(T_{wo})} \tag{2.16}$$

From this, the mass flow rate of water vapor at the outlet of the wet channel can be determined.

$$\dot{m}_{v,wo} = \omega_{wo} \dot{m}_{da,wo} = \omega_{wo} (1 - r_m) \dot{m}_{da,di} \tag{2.17}$$

The overall energy balance with the assumption of adiabaticity of the heat exchanger to the surroundings is finally expressed as

$$\begin{aligned} &\dot{m}_{da,di} c_{p,da} T_{di} + \dot{m}_{v,di} \left(h_{lv} + c_{p,v} T_{di}\right) + \dot{m}_l c_l T_l \\ &= \dot{m}_{da,p} c_{p,da} T_{do} + \dot{m}_{v,p} \left(h_{lv} + c_{p,v} T_{do}\right) + \dot{m}_{da,wo} c_{p,da} T_{wo} + \dot{m}_{v,wo} \left(h_{lv} + c_{p,v} T_{wo}\right) \end{aligned} \tag{2.18}$$

Within the equation of the overall energy balance, the mass flow rate of water vapor at the outlet of the wet channel is given by equation (2.17), and from this value, the mass flow rate of consumed liquid water can be inferred through equation (2.15). The temperature of the injected liquid water can be considered equal to the ambient temperature and thus equal to the inlet temperature $T_{di}$. With these assumptions in place, the system can be solved numerically to determine the outlet temperature of the wet channel and the amount of water consumed. The equivalent

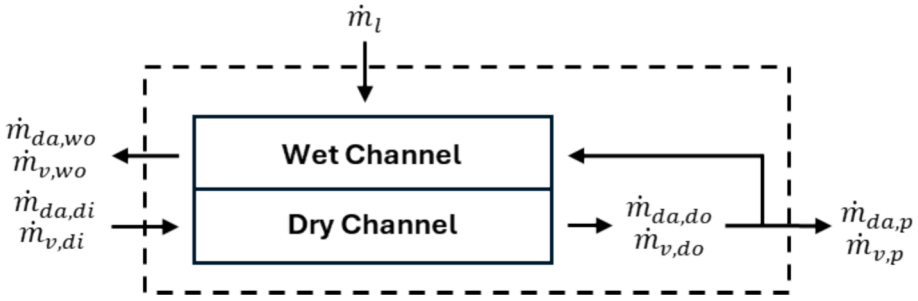


**Fig. 3.** M-cycle scheme for global mass and energy balances.

specific heat of the wet air mixture can be derived from the relationship

$$\dot{m}_{da}c_{p,da} + \dot{m}_{v}c_{p,v} = \dot{m}c_{p,eq} \tag{2.19}$$

$$\left(\dot{m}_{da} + \dot{m}_{v}\right)\frac{\dot{m}_{da}c_{p,da} + \dot{m}_{v}c_{p,v}}{\dot{m}_{da} + \dot{m}_{v}} = \dot{m}c_{p,eq}c_{p,eq} = \frac{\dot{m}_{da}c_{p,da} + \dot{m}_{v}c_{p,v}}{\dot{m}_{da} + \dot{m}_{v}} \tag{2.20}$$

By imposing a set point temperature for the room to be cooled, it is possible to calculate the cooling capacity of the M-cycle and determine, based on environmental conditions, how much thermal load can be absorbed. A quick estimate can be calculated using the relationship

$$\dot{Q}_{cool} = \dot{m}_{p}c_{p,eq,p}\left(T_{room} - T_{p}\right) \tag{2.21}$$

The mass flow rate of the wet air mixture at the outlet of the wet channel $\dot{m}_{v,wo}$ is calculated by summing the respective partial flow rates of dry air and vapor

$$\dot{m}_{wo} = \dot{m}_{da,wo} + \dot{m}_{v,wo} \tag{2.22}$$

The volumetric flow rate of the wet air mixture at the outlet of the wet channel can thus be calculated as

$$\dot{V}_{wo} = \frac{\dot{m}_{wo}}{\rho_{wo}} \tag{2.23}$$

where the density is once again determined using the procedure previously employed for the two preceding calculation stations.

In Table 1 the operating conditions and performance of the M-cycle are reported. It is observed that, both in the arid and tropical climates, the temperature of the working air exiting the wet channel ($T_{wo}$) exceeds the setpoint temperature of the classroom. This supports the decision to introduce exhaust air from the classroom into the ventilation channel, which is assumed to be at 27 °C. The $T_{do}$, on the other hand, consistently stays below the room's setpoint temperature, enabling heat extraction through the M-cycle under all climatic conditions.

### 2.3. Performance analysis

The analysis includes a preliminary assessment of the cooling capacity provided by the M-cycle, comparing it with the thermal load generated by the classroom occupants. A more detailed analysis could involve all the surfaces of the classroom; however, the aim here is not to perform a full energy analysis of the entire building but to calculate the differential advantage that the integration of a M-cycle cooling with the roof ventilation could offer.

Along with the psychrometric approach, the analysis employs a *CFD* method in which a channel of length $L_c = 7.2m$, height $d_c = 0.1m$, and unit depth was modelled through *OpenFOAM CFD* software [37]. The channel operates with a constant airflow rate, and the resulting air outlet temperatures, along with the thermal fluxes entering the structure through the ceiling, are determined for different scenarios and M-cycle operating conditions. The following subsections outline, respectively, the analytical approach used to define the boundary conditions for each scenario and the *OpenFOAM* model employed to calculate the heat transferred to the airflow and the ceiling of the classroom.

**Table 1**
M-cycle operating conditions and performance.

| | $T_a[^\circ C]$ | $T_{a,wb}[^\circ C]$ | $T_{wo}[^\circ C]$ | $T_{do}[^\circ C]$ |
|---|---|---|---|---|
| Arid | 42 | 21 | 29.7 | 18.7 |
| Temperate | 37 | 19 | 26.9 | 17.2 |
| Continental | 31 | 20 | 24.6 | 19.0 |
| Sub-tropical | 33 | 23 | 26.0 | 22.3 |
| Tropical | 33 | 26 | 28.3 | 25.3 |

#### 2.3.1. Definition of the boundary conditions

The cavity outer layer is exposed to a mixed radiative-convective condition since incident solar radiation is assumed $I = 780\frac{W}{m^2}$ and the presence of wind ($w_{wind} = 1\frac{m}{s}$) is considered.

This heat transfer boundary condition can be simulated through a fully convective condition by considering a single-dimension heat flux through the wall and by calculating an equivalent radiative-convective heat transfer coefficient ($h_e$) as described in ref. [38] and reported in Eq. (2.24), along with the calculation of an equivalent undisturbed flow temperature referred to as the *sol–air temperature* ($T_{s/a}$)

$$R_{h,e} = \frac{1}{h_e} = \frac{1}{h_{ce} + h_r} = \frac{1}{(4 + 4w_{wind}) + \epsilon\sigma_0 4T_{me}^3} \tag{2.24}$$

where $R_{s,e}$ is the thermal resistance of the outer slab, $h_{ce}$ is the convective heat transfer coefficient calculated through the wind speed and $h_r$ is the radiative heat transfer coefficient calculated through the outer surface thermal emittance ($\epsilon$), the Stefan-Boltzmann constant ($\sigma_0 = 5.67{\cdot}10^{-8}\frac{W}{m^2K^4}$) and $T_{me}$ is the thermodynamic mean equivalent temperature (in kelvin), which can be estimated according to Eq. (2.25). An iterative calculation was therefore applied to $T_{me}$ to account for the variation in $T_{s,e}$.

$$T_{me} = \frac{T_{sky} + T_{s,e}}{2} \tag{2.25}$$

An external air temperature ($T_e$) can thus be defined taking into consideration the convective heat transfer coefficient calculated through Eq. (2.24).

$$T_e = \frac{h_r T_{sky} + h_{ce} T_a}{h_e} \tag{2.26}$$

$T_{sky}$ is the sky temperature, while $T_a$ is the external air ambient temperature (dry bulb), variable according to the simulated climate zones reported in Section 2.1.

The equivalent air temperature such as to produce, by convection alone, the effect that would be obtained by adding radiation to wind convection. In the exposed conditions, the equivalent temperature is the already mentioned sol–air temperature and is calculated using Eq. (2.27).

$$T_{s/a} = T_e + R_{h,e}\alpha I \tag{2.27}$$

According to this calculation, the convective boundary condition can be applied to the outer layer external surface by considering an equivalent ambient temperature $T_{s/a}$ and an equivalent convective heat transfer coefficient $h_e$.

The conduction through the solid outer layer is modelled through a conductive heat transfer resistance $R_{ke}$, as described in equation (2.28), which has to be added to $R_{h,e}$ to obtain the total thermal resistance of the outer roof layer.

$$R_{ke} = \frac{d_e}{\lambda_e} \tag{2.28}$$

The inner layer is modelled by creating an equivalent radiative-convective thermal resistance between the room and the internal surface of the slab ($R_{h,i}$), and a conductive resistance ($R_{ki}$) that operates within the slab thickness. In this case, the heat transfer by radiation between the surface and the room was neglected.

$$R_{h,i} = \frac{1}{h_i} \quad where \quad h_i = 6\frac{W}{m^2K} \tag{2.29}$$

$$R_{ki} = \frac{d_i}{\lambda_i} \tag{2.30}$$

In Fig. 4 is reported the thermal resistance scheme of the solid walls in

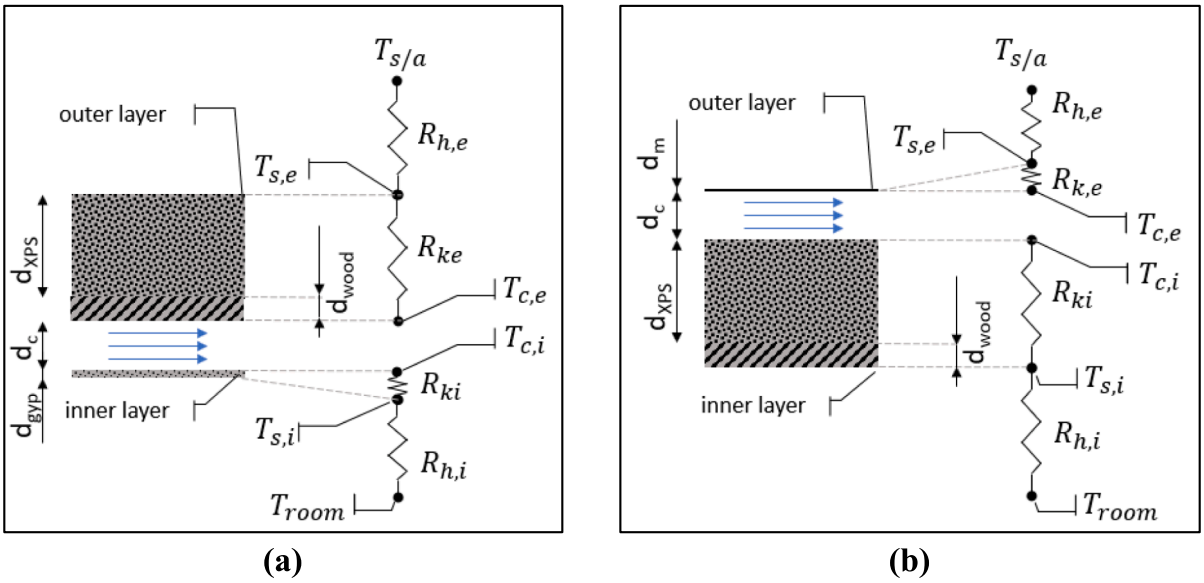


**Fig. 4.** Equivalent thermal resistance of the cavity at bottom (a) and cavity at top (b) tested configurations.

the different cavity positions.

*2.3.2. OpenFOAM model*

The steady-state thermofluid-dynamics simulations were conducted using the *OpenFOAM* solver, *buoyantSimpleFoam*, a steady-state solver for turbulent flow of compressible fluids, validated in ventilation and heat-transfer fields. This solver calculates the temperature increase of the air as it moves through the channel and determines the heat fluxes through the adjacent walls. The computational domain was modelled in 2D, discretizing the channel along its length and height, with a unitary cell depth. Fig. 5 schematically illustrates the boundaries of the computational domain, as briefly described below:

- Inlet: the channel inlet is represented as a fixed value temperature and velocity inlet with uniform profile. The fluid inlet velocity ($u_{in}$) was calculated through an average working air volumetric flow rate $\dot{V}_{wo}$ and the cross-sectional area of the roof channels spanning 0.1 m in height and 6.8 m in width per classroom, for a total of 3 classrooms. For instance, $u_{in} = 0.369 \frac{m}{s}$ in the cases where the channel is ventilated with working air and external air, while $u_{in} = 0.225 \frac{m}{s}$ when exhaust air is introduced, since the volumetric flow rates of working and exhaust air are respectively 2595 $\frac{m^3}{h}$ and 1650 $\frac{m^3}{h}$.

For the exhaust air, the minimum value required by regulations was conservatively considered (higher values would improve the performance of the ventilated roof), acknowledging that when air renewal is performed through the product air of the M-cycle, significantly higher flow rates are achieved.

- Outlet: the outlet is represented with a *zeroGradient* boundary condition for both velocity and temperature, as re-entrant flows are not considered due to the forced ventilation scenario.
- Outer and inner walls: these patches are defined through the *externalWallHeatFluxTemperature* boundary condition which applies a heat flux condition on an external wall through a fixed freestream temperature and a specified convective heat transfer coefficient (other options such as fixed heat transfer rate and fixed heat flux are available). When the convective condition is selected, it also allows the simulation of the surface as a series of thermal resistances by specifying the layer thickness and the material thermal conductivity.

The steady-state model represents an approximation of almost-steady-state behavior, reasonable for a lightweight roof structure as considered. In particular, it is expected that the heat transfer coefficients are satisfactorily calculated.

In the absence of an experimental setup replicating the simulated model of forced convection, the validation of the solver was carried out by referencing similar configurations available in the literature related to naturally ventilated pitched roofs, adapting the model to these conditions. Specifically, data from Susanti et al. [39] were used, which describe a cavity model (4882 mm × 400 mm × 78 mm) heated on its upper surface to simulate solar radiation on a roof. The heating is achieved using electric heating plates embedded in the upper structure of the cavity along its length. These plates were simulated in the numerical model using the *flux* function of the *externalWallHeatFluxTemperature* boundary condition.

This experimental configuration is particularly relevant since the upper surface of the cavity was covered with aluminum foil to reduce radiation from the surface. This simplification aligns with the CFD model, which does not account for radiative heat transfer. A test condition with a heat production of 100 W/m$^2$ was selected, leading to an average velocity in the channel of 0.25 m/s, the closest match to the numerical model conditions for which sufficient data were available. The lower surface of the cavity consists of a 12 mm thick plywood board and a 50 mm thick polystyrene foam sheet. These elements were accounted for in the model to determine the total conductive resistance, and a convective resistance was introduced on the lower surface exposed to the environment, assuming $h_i = 6 \frac{W}{m^2 K}$. The paper does not specify the ambient temperature, which could introduce errors in the assessment of heat dissipation. However, an ambient temperature of 20 °C was assumed, as the experimental tests were conducted inside a laboratory.

For validation, the temperature trends of the upper and lower surfaces of the channel were compared with those reported in Susanti et al.'s experiment, as presented in Section 3.1.

## 3. Results

### 3.1. CFD model validation

Fig. 6 compares the top and bottom surface temperatures of the cavity, showing the overall agreement between numerical and experimental results under the conditions described by Susanti et al. The calculated top surface temperatures closely match the experimental

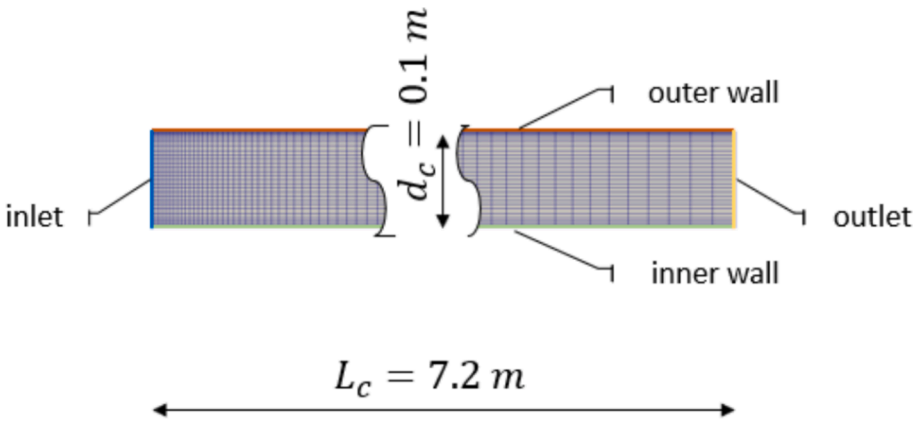


**Fig. 5.** Schematic representation of the discretized 2D computational domain.

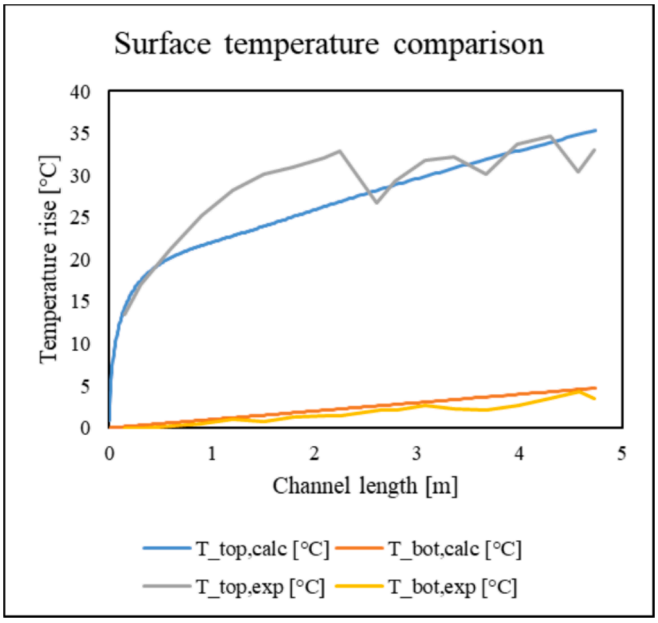


**Fig. 6.** Comparison between experimental (exp) and numerical (*calc*) trends of the upper ($T_{top}$) and lower ($T_{bot}$) surface temperatures of the cavity.

values in the final sections of the channel, with deviations generally remaining within acceptable limits, averaging below ± 5 %. However, a discrepancy is observed between 0.5 m and 2.5 m where this divergence may be attributed to localized effects in the experimental setup, such as non-uniformities in the heat flux distribution due to the uneven placement of heaters (as also stated by the authors). These effects seem to be further evidenced by surface temperature fluctuations from the midpoint of the channel onward. Since the numerical model assumes a uniform heat flux, it may not fully capture these localized variations, contributing to the observed differences.

For the bottom surface, deviations are minimal, indicating that the model accurately represents the dominant thermal phenomena for this surface and provides a reliable estimate of the heat transferred to the indoor environment.

### 3.2. Ventilated roof performance comparison

Fig. 7 reports the results of the equivalent convective heat transfer coefficient and the sol–air temperature used as convective boundary condition for the outer surface in the *OpenFOAM* model. The cases are described according to the nomenclature A-B-C-D where *15, 10* or *5* refer to the insulating material thickness (in cm), 2.5 refers to the woody layer thickness, 1.2 to the drywall thickness, 0.1 to the metal sheet thickness and *a* to the position of the channel between the layers.[1]

The considered solar irradiance leads to equivalent air temperature that varies through the different roof configuration according to the iteratively calculated external surface temperature ($T_{s,e}$), and ranges between 52.3 °C and 61.8 °C with higher values observed in the arid climate and in cases with greater insulation thickness, in both the *cavity at bottom* and *cavity on top* configurations. The convective heat transfer coefficient $h_c$ and the equivalent radiant coefficient $h_r$ almost equally contribute to the formation of $h_e$, which is nearly constant over the tested conditions ranging between 14.1 and 14.5 $\frac{W}{m^2K}$. It is observed that for those scenarios where ventilation is realized with external air, the subtropical and tropical cases were consolidated into a single category due to the same dry-bulb temperature and the minimal variation in equivalent specific heat.

The complete dataset is shown in Table A.1 in the Appendix A.

Fig. 8 shows the averages inlet and outlet temperatures of the air in the ventilation channel. As highlighted more clearly in Table A.1, only in cases with the *cavity at bottom* configuration operating in continental climate (characterized by low ambient temperature and low relative humidity) and provided with 15 cm and 10 cm of roof insulation (15–2.5-a-1.2 and 10–2.5-a-1.2), the air temperature within the channel consistently remain below the room's setpoint temperature contributing to the active cooling of the environment below regardless of the stratification of the fluid along the height of the channel.

In the other cases, the average air temperature at the channel outlet exceeds the room setpoint temperature (27 °C). This suggests that, beyond a certain channel length, the bottom surface of the cavity may rises above the setpoint, potentially compromising its role in actively cooling the room. If we consider, for example, the case of *cavity on top* (0.1-a-15–1.2) ventilated with working air under continental climate conditions, the inlet air temperature is 24.6 °C, while the average outlet temperature reaches 36.5 °C. Examining the temperature profiles reported in Fig. 9a, the air temperature near the bottom surface of the cavity remains below the setpoint up to a length of approximately 4 m measured from the channel inlet. As shown in Fig. 9b, the bottom surface temperature remains nearly equal to the inlet air temperature for the first 2 m, then increases almost linearly, reaching 32 °C at the outlet.

[1] E.g. *15–2.5-a-1.2* refers to the configuration *cavity at bottom*, where 15 cm of insulating material face the external environment, followed by 2.5 cm of wood, the channel, and 1.2 cm of drywall facing the internal environment.The *cavity on top* configuration is instead represented by all cases starting with *0.1-a-xx-2.5*, where *0.1* indicates a metal sheet layer, *a* specifies the channel's position below followed by the insulating material (*xx* thickness) and the wood decking.

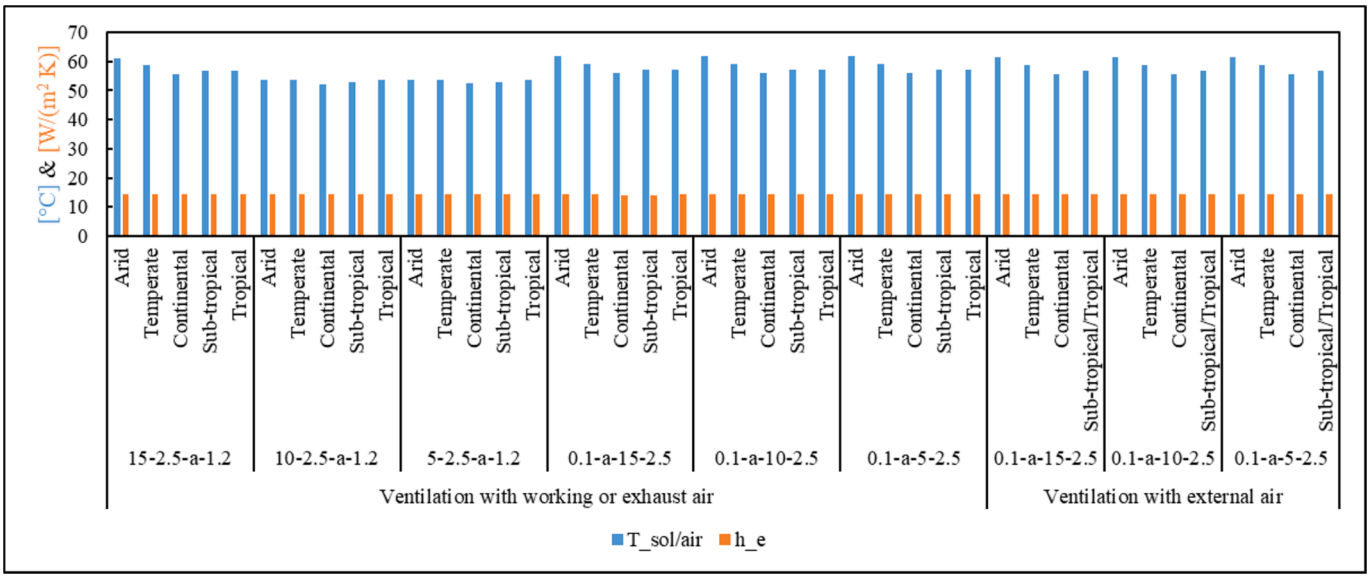


**Fig. 7.** Calculated values of the sol/air temperature and of the equivalent heat transfer coefficient based on the different climates and different rooftop configurations.

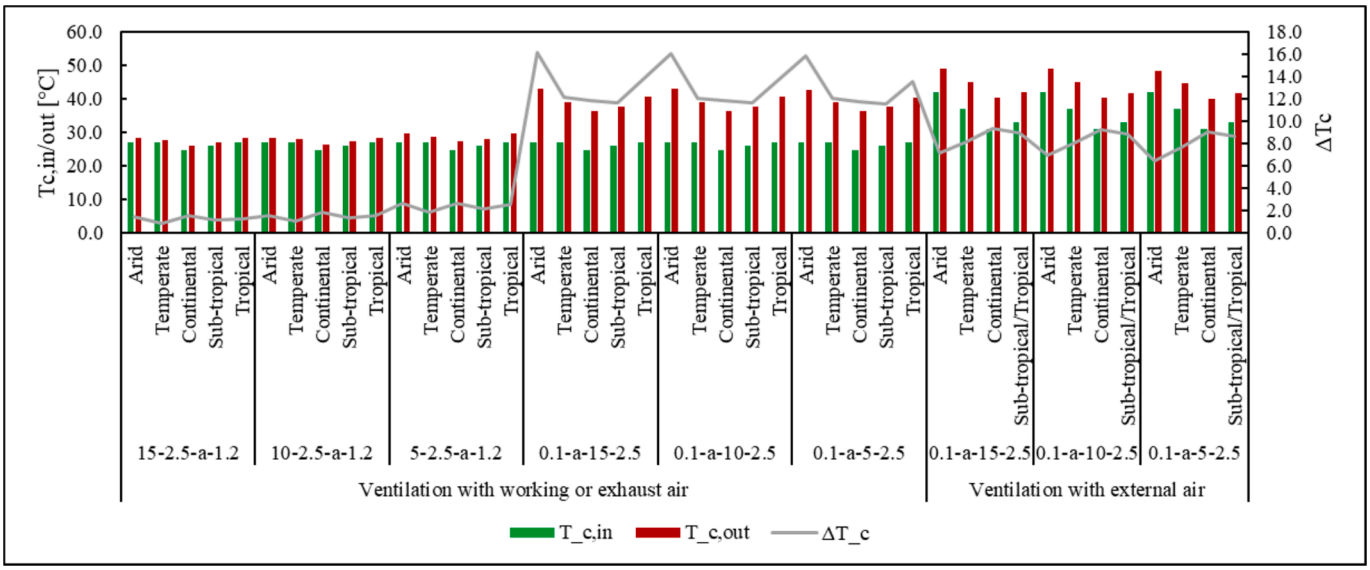


**Fig. 8.** Ventilated roof inlet ($T_{c,in}$) and outlet ($T_{c,out}$) temperatures at different scenarios. For convenience, the temperature difference ($\Delta T_c$) is also reported.

The channel length is, therefore, a critical parameter for tuning these systems, as reported in previous work by Pedrazzi et al. [31]. Alternative strategies, paying in terms of complexity, could involve splitting the cooling airflow to introduce fresh air from the midpoint of the channel onward. This approach could be effective if temperature stratification remains significant. However, halving the flow rate would lead to a laminar regime, requiring additional simulations to assess its feasibility and effectiveness.

Regarding the calculation of the thermal flux transmitted to the indoor environment, the results are presented in the graphs of Fig. 10, where the average heat fluxes (considered positive when directed from the cooled environment to the cavity) and ceiling surface temperatures are shown for the cases of ventilation with working air in the *cavity at bottom* configuration (a, b) and the *cavity on top* configuration (c, d). It is noted that for arid and tropical climates, exhaust air at $T_{in} = 27^{\circ} C$ was used instead of working air. Graphs (e, f) contain the results for the baseline configuration with the channel ventilated using external air at ambient temperature, while the following paragraphs provide insights into the cavity positioning and the chosen ventilation strategy.

*Impact of cavity position*

The impact of the cavity position confirms the results obtained in previous work [31] where a direct evaporative cooler was used. When the cavity is placed at bottom (e.g., 15–2.5-a-1.2), the insulation material directly facing the external environment significantly reduce heat transferr, and the thermal gradient experienced by the airflow is on average below 4 °C. Under these conditions, stratification plays a secondary role and this setup likely results in lower ceiling temperatures and heat flux into the room compared to the cavity on top configurations (0.1-a-xx-2.5), where the presence of the metal sheet at the top increases the heat flux, which is not totally offset by the airflow. In this last condition, in fact, the average thermal gradient experienced by the air is around 25 °C, as shown in Fig. 9a, and the stratification, which tends to dissipate from the midpoint of the channel onward, influences the result as usually happens in naturally ventilated pitched roofs.

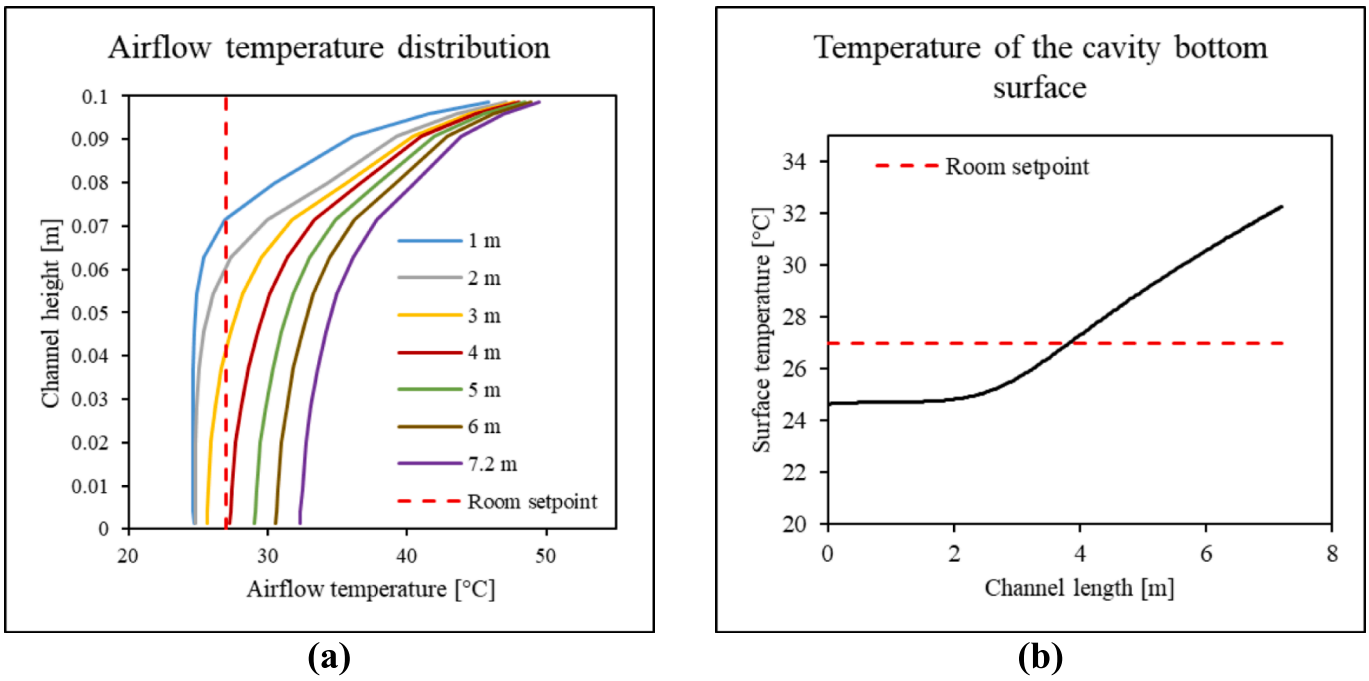


**Fig. 9.** Representation of the temperature profiles on the channel section at different distances from the inlet (a) and representation of the trend of the lower surface temperature of the ventilated cavity (b) for the case (0.1-a-15–1.2) ventilated with working air in continental climate.

In optimal M-cycle operating conditions, particularly in a continental and sub-tropical climates, relocating the cavity to the bottom results in a thermal flux reduction of two orders of magnitude with the ceiling that acts as a radiant cooling surface, effectively removing heat from the classroom. As a secondary effect, having a low ceiling temperature reduces the so-called "hot head effect" (i.e., the discomfort perceived when the head is warmed by a hot ceiling surface through far-infrared radiation), thereby improving overall thermal comfort.

Considering the total roof surface area of the three classrooms, this translates into a reduction in the heat transfer rate to the indoor environment of 637 W, 624 W, and 578 W for insulation thicknesses of 15 cm, 10 cm, and 5 cm, respectively. Similar reductions are observed in a subtropical climate, with an average decrease of around 270 W. In other climatic conditions, the reduction in total transmitted thermal power averages around 66 W.

From another perspective, the *cavity at bottom* configuration with only 5 cm of insulating material (5–2.5-a-1.2) outperforms the *cavity on top* configuration with 15 cm of insulation (0.1-a-15–2.5). This suggests alternative strategies to heavy insulation, particularly for buildings operating in mild winter conditions.

*Impact of ventilation strategies*

When comparing the *cavity on top* configuration ventilated with working or exhaust air versus external air (Fig. 10 (c) and (e)), the results, as expected, clearly favor the use of working or exhaust air. The total thermal power transferred to the indoor environment reaches a peak of 1045 W in an arid climate with 5 cm of insulation (0.1-a-5–2.5) and ventilation using external air at ambient (42 °C) temperature. In the same scenario, ventilating with exhaust air results in a 68 % reduction in heat flux, corresponding to a decrease of 710 W. The reduction remains significant across all other cases as well. The thermal flux achieved with the *cavity on top* configuration ventilated with exhaust air and 5 cm of insulation (0.1-a-5–2.5 in Fig. 10c) is comparable to that obtained by ventilating the *cavity on top* with external air and 15 cm of insulation (0.1-a-15–2.5 in Fig. 10e). In the analysed cases, simply recovering and reusing the exhaust air from the room would allow for a two-thirds reduction in insulation material, resulting in a roof that can benefits more effectively from nighttime cooling.

### 3.3. Cooling capacity assessment and efficiency gains from M-cycle and ventilated roof integration

For the presented case study, with a floor area of approximately 50 $m^2$, regulations indicate a maximum occupancy of 22 people, resulting in a metabolic heat load of about 2.8 kW. The required ventilation airflow, as per the relevant standards, is approximately 550 $m^3$/h. However, the product air flow generated by the M-cycle can handle significantly higher airflows. Specifically, considering a product air flow rate of 3546 $m^3$/h, the available airflow per classroom is increased to 1182 $m^3$/h, in order to enhance the cooling capacity for each environment. Under these conditions, the cooling capacity ($\dot{Q}_{cool}$) reported in Table 2 varies significantly depending on the considered climate, ranging from a minimum of 2 kW in tropical climates to a maximum of 11.8 kW in continental climates. It can be observed that, excluding tropical and sub-tropical climates, where high humidity levels in the air lowers the performance of evaporative cooling systems, the selected M-cycle machine can handle the metabolic heat load ($\dot{Q}_{met}$) generated by fully occupied classrooms with a surplus of 40 % in the case of a continental climate (see the $\frac{\dot{Q}_{cool}}{\dot{Q}_{met}}$ ratio in Table 2).

Assuming a constant electrical power consumption of $\dot{L}_e = 1800$ W for the M-cycle cooler, operating under maximum pressure drop conditions and with energy entirely used by the fans processing both product and working air, the EER of the M-cycle cooler can be calculated as $EER = \frac{\dot{Q}_{cool}}{\dot{L}_e}$ and the results are reported in Table 2 according to the different climatic conditions. The results show that the EER varies between 1.1 and 6.5, confirming that this solution is not optimal for tropical climates, where exhaust air was, in fact, chosen to ventilate the cavity. On the other hand, in arid climates the EER is high but the temperature of the working air exceeds the room setpoint (see Table 1), making it unsuitable for cavity ventilation, which was therefore achieved again with exhaust air. In these two cases, however, the possibility of using the working air (colder than the ambient) to cool the condenser of the VCR system would lead to an increase of its EER.

When operating in temperate, continental, or subtropical climates and combining the M-cycle cooler with a ventilated roof, the possibility

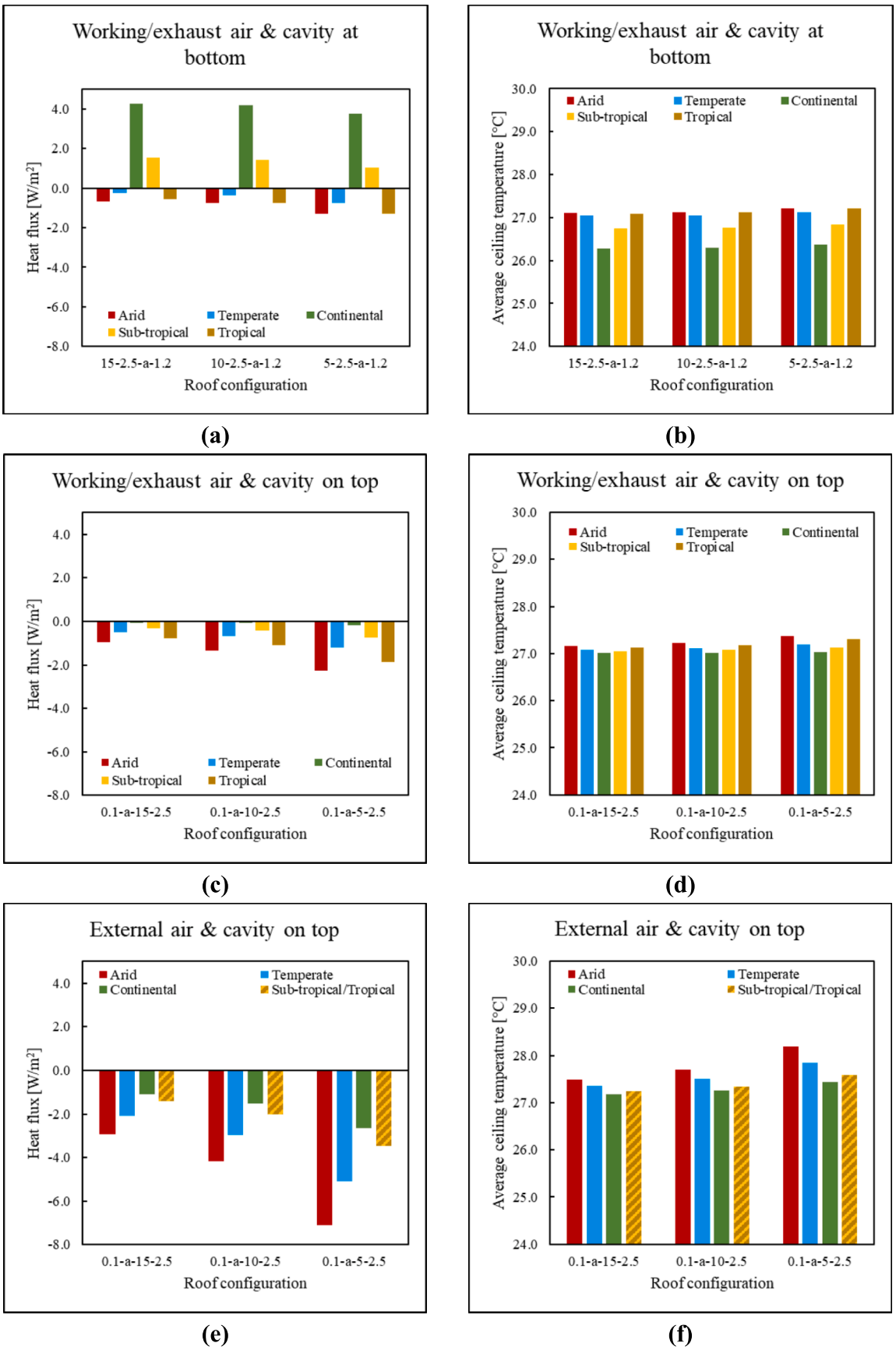


**Fig. 10.** Heat flux and average ceiling temperature for each tested configuration.

**Table 2**
M-cycle room cooling capacity.

| | $T_{DB,di}[^\circ C]$ | $T_{WB,di}[^\circ C]$ | $T_{do}[^\circ C]$ | $\dot{Q}_{cool}[kW]$ | $\dot{Q}_{cool}/\dot{Q}_{met}$ | $EER$ |
|---|---|---|---|---|---|---|
| Arid | 42 | 21 | 18.7 | 9.9 | 1.2 | 5.5 |
| Temperate | 37 | 19 | 17.2 | 11.8 | 1.4 | 6.5 |
| Continental | 31 | 20 | 19.0 | 9.5 | 1.1 | 5.3 |
| Sub-tropical | 31 | 23 | 22.3 | 5.6 | 0.7 | 3.1 |
| Tropical | 33 | 26 | 25.3 | 2.0 | 0.2 | 1.1 |

of recovering the working air allows for an estimation of a combined EER. This is obtained by summing the sensible cooling effect from using the product air for room ventilation with the reduction of external heat gain due to cavity ventilation with working air.

By comparing identical roof stratigraphy, replacing external air with working air in the cavity-on-top configuration results in a reduction of the thermal power transmitted through the roof, ranging from 150 W to 572 W for the total roof surface area of the three considered classrooms. Fig. 11 reports the reduction in thermal power achieved with this technological solution for different insulation thicknesses, highlighting an increasing benefit when ventilating the roof with working air as the insulation thickness decreases.

Focusing on the less insulated tested roof (0.1-a-5–2.5) and summing the reduction in transmitted thermal power with the cooling contribution provided by the product air used for ventilation, the combined EER increases by 7.1 %, 3.8 %, and 4.9 % compared to the EER of the M-cycle cooler alone, for subtropical, continental, and temperate climates, respectively.

## 4. Conclusions

This study presents a preliminary analysis of the coupling between an M-cycle evaporative cooler and a ventilated roof to enhance both energy efficiency and indoor thermal comfort, considering the necessary requirements for school buildings. It has been demonstrated that the product air from the M-cycle not only ensures proper air exchange but also contributes to cooling the indoor environment, effectively reducing the thermal load on VCR systems. However, it is important to note that the EER value is strongly dependent on climatic conditions, with the minimum value being 1.1 in tropical climates, where the application of this solution does not seem to be feasible.

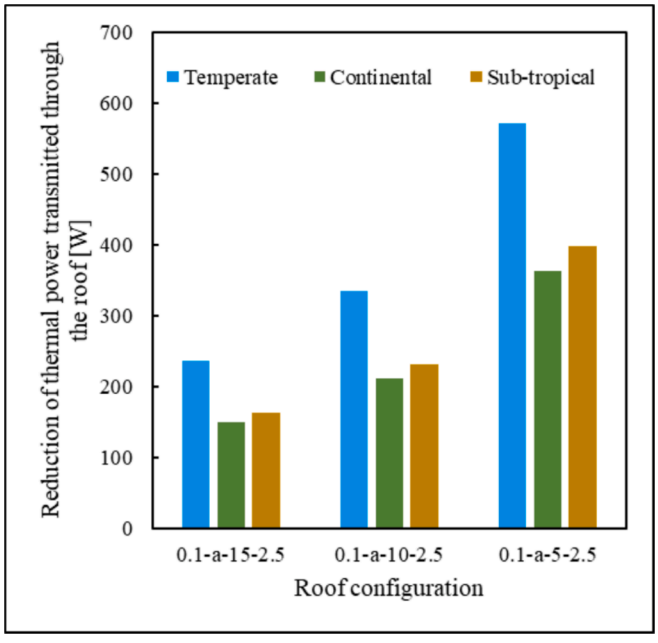


**Fig. 11.** Reduction of thermal loads from the roof when comparing ventilation with working air versus external air.

In this regard, an extension of the EER of the M-cycle has been proposed, also accounting for the reduced solar gain due to the use of the working air to ventilate the cavity. In subtropical continental and temperate climates, a cooling capacity increase ranging from 3.8 % to 7.1 % is achieved, contributing to an equivalent increase in the EER.

The impact of cavity positioning in these forced ventilated roofs is also significant, with the cavity at bottom outperforming the cavity on top in terms of heat transfer reduction, maintaining a low thermal gradient of the air (perpendicular to the airflow direction) of around 4 °C, compared to the top cavity, where the thermal gradient reaches up to 25 °C and buoyant stratification becomes crucial. The cavity at bottom configuration achieves in fact heat flux reductions of two orders of magnitude in continental and subtropical climates and one order of magnitude in other climates.

The study also highlights the effectiveness of ventilation strategies, especially when using exhaust or working air to ventilate the cavity. In an arid climate with 5 cm of insulation, ventilating through the exhaust air reduces the thermal flux by two-thirds compared to using ambient air at 42 °C. In tropical climates, the reduction is 45 %, and in temperate climates, it can reach up to 94 %. The bottom cavity configuration with only 5 cm of insulation achieves comparable thermal performance to a top cavity configuration with 15 cm of insulation, showcasing the potential for reducing insulation needs while enhancing cooling performance and thermal comfort.

## 5. Future works

The work carried out so far provides general guidelines on the integration of an M-cycle in a building with the goal of using waste humid air to ventilate a horizontal roof. The school environment was referenced in order to set some boundary conditions through the use of regulations, however, this approach can be extended to any similar civil or industrial application.

It is also important to underline that the steady-state model can be a strong approximation in certain conditions, whereas a more detailed and accurate analysis could certainly be carried out through the implementation of a dynamic simulation. This recommendation for future work would allow for the investigation of more massive roofs with different stratigraphies than those studied so far, broadening the range of case studies. Furthermore, the consideration of using a VCR to maintain a fixed room setpoint temperature simplified the calculations but shifts the focus to the operating conditions of the VCR, which should be investigated in terms of seasonal average EER with dynamic analysis.

This approach would allow a detailed economic analysis that should be used to evaluate the instantaneous cooling cost for both the VCR and the M-cycle. For the latter, it is thus essential to consider not average conditions divided by climate zones but hourly conditions, assessing the variation of dry and wet bulb temperature throughout the day.

## CRediT authorship contribution statement

**Nicolò Morselli:** Writing – original draft, Methodology, Investigation, Conceptualization. **Marco Puglia:** Writing – review & editing, Methodology, Conceptualization. **Michele Cossu:** Writing – original draft, Methodology, Investigation, Conceptualization. **Simone**

**Pedrazzi:** Writing – review & editing, Methodology. **Giulio Allesina:** Writing – review & editing, Methodology. **Paolo Tartarini:** Supervision. **Alberto Muscio:** Supervision, Methodology, Conceptualization.

## Declaration of competing interest

The authors declare that they have no known competing financial interests or personal relationships that could have appeared to influence the work reported in this paper.

## Acknowledgment

Project funding: avviso pubblico per la presentazione di Proposte di intervento per la creazione e il rafforzamento di "ecosistemi dell'innovazione", costruzione di "leader territoriali di R&S" – Ecosistemi dell'Innovazione – nell'ambito del Piano Nazionale di Ripresa e Resilienza, Missione 4 Istruzione e ricerca – Componente 2 Dalla ricerca all'impresa – Investimento 1.5, finanziato dall'Unione europea – NextGenerationEU- DD. 3277/2021. Ecosystem For Sustainable Transition of Emilia-Romagna (ECOSISTER): CUP: E93C22001100001.

## Appendix A

### *A.1. Simulation results and dataset*

.

**Table A.1**
Dataset of the results.

| Roof configuration | Climate zone | $T_{\frac{sol}{air}}$ [°C] | $h_e\left[\frac{W}{m^2}\right]$ | $T_{c,in}$ [°C] | $T_{c,out}$ [°C] | $\Delta T_c$ [°C] | $\dot{q}\left[\frac{W}{m^2}\right]$ |
|---|---|---|---|---|---|---|---|
| 15–2.5-a-1.2 | Arid | 61.17 | 14.54 | 27.0 | 28.4 | 1.4 | −0.67 |
| | Temperate | 58.64 | 14.45 | 26.9 | 27.8 | 0.9 | −0.27 |
| | Continental | 55.53 | 14.35 | 24.6 | 26.2 | 1.6 | 4.28 |
| | Sub-tropical | 56.57 | 14.38 | 26.0 | 27.2 | 1.2 | 1.53 |
| | Tropical | 56.58 | 14.37 | 27.0 | 28.2 | 1.2 | −0.58 |
| 10–2.5-a-1.2 | Arid | 53.55 | 14.4 | 27.0 | 28.6 | 1.6 | −0.74 |
| | Temperate | 53.55 | 14.3 | 26.9 | 28.0 | 1.1 | −0.35 |
| | Continental | 52.25 | 14.2 | 24.6 | 26.5 | 1.9 | 4.16 |
| | Sub-tropical | 53.05 | 14.2 | 26.0 | 27.4 | 1.4 | 1.42 |
| | Tropical | 53.55 | 14.2 | 27.0 | 28.6 | 1.6 | −0.74 |
| 5–2.5-a-1.2 | Arid | 53.65 | 14.4 | 27.0 | 29.6 | 2.6 | −1.28 |
| | Temperate | 53.55 | 14.3 | 26.9 | 28.8 | 1.8 | −0.74 |
| | Continental | 52.35 | 14.2 | 24.6 | 27.3 | 2.6 | 3.77 |
| | Sub-tropical | 53.05 | 14.2 | 26.0 | 28.2 | 2.1 | 1.03 |
| | Tropical | 53.65 | 14.2 | 27.0 | 29.6 | 2.6 | −1.28 |
| 0.1-a-15–2.5 | Arid | 61.75 | 14.31 | 27.0 | 43.2 | 16.2 | −0.94 |
| | Temperate | 59.22 | 14.2 | 26.9 | 39.1 | 12.2 | −0.48 |
| | Continental | 56.03 | 14.12 | 24.6 | 36.5 | 11.9 | −0.06 |
| | Sub-tropical | 57.09 | 14.15 | 26.0 | 37.7 | 11.7 | −0.30 |
| | Tropical | 56.98 | 14.2 | 27.0 | 40.8 | 13.8 | −0.78 |
| 0.1-a-10–2.5 | Arid | 61.65 | 14.4 | 27.0 | 43.1 | 16.1 | −1.33 |
| | Temperate | 59.15 | 14.3 | 26.9 | 39.0 | 12.1 | −0.69 |
| | Continental | 55.95 | 14.2 | 24.6 | 36.4 | 11.8 | −0.09 |
| | Sub-tropical | 56.95 | 14.2 | 26.0 | 37.7 | 11.6 | −0.43 |
| | Tropical | 56.95 | 14.2 | 27.0 | 40.7 | 13.7 | −1.11 |
| 0.1-a-5–2.5 | Arid | 61.65 | 14.4 | 27.0 | 42.8 | 15.8 | −2.28 |
| | Temperate | 59.15 | 14.3 | 26.9 | 38.9 | 12.0 | −1.20 |
| | Continental | 55.95 | 14.2 | 24.6 | 36.4 | 11.8 | −0.16 |
| | Sub-tropical | 56.95 | 14.2 | 26.0 | 37.6 | 11.6 | −0.75 |
| | Tropical | 56.95 | 14.2 | 27.0 | 40.5 | 13.5 | −1.89 |
| 0.1-a-15–2.5 | Arid | 61.25 | 14.5 | 42.0 | 49.2 | 7.2 | −2.94 |
| | Temperate | 58.75 | 14.4 | 37.0 | 45.2 | 8.2 | −2.10 |
| | Continental | 55.65 | 14.3 | 31.0 | 40.3 | 9.3 | −1.08 |
| | Sub-tropical/Tropical | 56.75 | 14.3 | 33.0 | 42.0 | 9.0 | −1.42 |
| 0.1-a-10–2.5 | Arid | 61.25 | 14.5 | 42.0 | 49.0 | 7.0 | −4.16 |
| | Temperate | 58.75 | 14.4 | 37.0 | 45.0 | 8.0 | −2.97 |
| | Continental | 55.65 | 14.3 | 31.0 | 40.3 | 9.3 | −1.54 |
| | Sub-tropical/Tropical | 56.75 | 14.3 | 33.0 | 41.9 | 8.9 | −2.02 |
| 0.1-a-5–2.5 | Arid | 61.25 | 14.5 | 42.0 | 48.5 | 6.5 | −7.11 |
| | Temperate | 58.75 | 14.4 | 37.0 | 44.7 | 7.7 | −5.09 |
| | Continental | 55.65 | 14.3 | 31.0 | 40.1 | 9.1 | −2.64 |
| | Sub-tropical/Tropical | 56.75 | 14.3 | 33.0 | 41.6 | 8.6 | −3.46 |

### *A.2. Energy balance of the CFD model*

Fig. A.1 Shows the result of the heat transfer rate balance for the ventilated channel system obtained from the simulations using *OpenFOAM*. The deviations are on average 1 %, with maximum peaks of up to 4 %. The graph shows the lines at ±5 %.

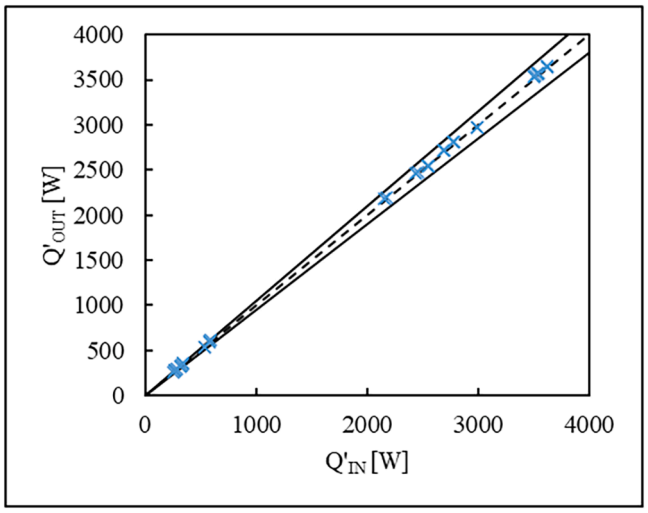


**Fig. A.1.** Thermal power entering and leaving the computational domain.

## Data availability

Data will be made available on request.

## References


[1] International Energy Agency, *The Future of Cooling*. IEA, 2018. [Online]. Available: https://www.iea.org/reports/the-future-of-cooling.

[2] Administration U. S. Energy Information, "Use of electricity." [Online]. Available: https://www.eia.gov/energyexplained/electricity/use-of-electricity.php.

[3] Y. Al horr, M. Arif, M. Katafygiotou, A. Mazroei, A. Kaushik, E. Elsarrag, Impact of indoor environmental quality on occupant well-being and comfort: a review of the literature, Int. J. Sustain. Built Environ. 5 (1) (2016) 1–11, https://doi.org/10.1016/j.ijsbe.2016.03.006.

[4] Energy U. S. Department of Energy, "Quadrennial Technology Review 2015," 2015. [Online]. Available: https://www.energy.gov/quadrennial-technology-review-2015.

[5] W. J. Fisk, "Review of Health and Productivity Gains From Better IEQ," 2000.

[6] J.M. Daisey, W.J. Angell, M.G. Apte, Indoor air Quality, Ventilation And Health Symptoms In Schools: An Analysis Of Existing Information, Blackwell Munksgaard, 2003, 10.1034/j.1600-0668.2003.00153.x.

[7] R.J. De Dear, et al., Progress in thermal comfort research over the last twenty years, Indoor Air 23 (6) (2013) 442–461, https://doi.org/10.1111/ina.12046.

[8] I. Sarbu, C. Pacurar, Experimental and numerical research to assess indoor environment quality and schoolwork performance in university classrooms, Build. Environ. 93 (P2) (2015) 141–154, https://doi.org/10.1016/j.buildenv.2015.06.022.

[9] O. A. Seppänen, S. Seppänen, W. J. Fisk, and M. J. Mendell, "Association of Ventilation Rates and CO 2 Concentrations with Health and Other Responses in Commercial and Institutional Buildings," 1999.

[10] W. J. Fisk, "The ventilation problem in schools: literature review," Nov. 01, 2017. doi: 10.1111/ina.12403.

[11] R. Becker, I. Goldberger, M. Paciuk, Improving energy performance of school buildings while ensuring indoor air quality ventilation, Build. Environ. 42 (9) (2007) 3261–3276, https://doi.org/10.1016/j.buildenv.2006.08.016.

[12] Z. Duan, C. Zhan, X. Zhang, M. Mustafa, X. Zhao, B. Alimohammadisagvand, A. Hasan, Indirect evaporative cooling: past, present, and future potentials, Renew. Sustain. Energy Rev. 16 (9) (2012) 6823–6850, https://doi.org/10.1016/j.rser.2012.07.007.

[13] L. Gillan, "MAISOTSENKO CYCLE FOR COOLING PROCESSES," 2008.

[14] Z. Duan, C. Zhan, X. Zhao, X. Dong, Experimental study of a counter-flow regenerative evaporative cooler, Build. Environ. 104 (2016) 47–58, https://doi.org/10.1016/j.buildenv.2016.04.029.

[15] Z. Duan, X. Zhao, C. Zhan, X. Dong, H. Chen, Energy saving potential of a counter-flow regenerative evaporative cooler for various climates of China: Experiment-based evaluation, Energ. Buildings 148 (2017) 199–210, https://doi.org/10.1016/j.enbuild.2017.04.012.

[16] A. Muscio, et al., Enhancing energy-efficient thermal control in buildings with a hybrid M-cycle/vapor compression refrigeration system, in: U. Berardi (Ed.), Multiphysics and Multiscale Building Physics, Springer Nature Singapore, Singapore, 2025, pp. 91–96.

[17] M. Ciampi, F. Leccese, G. Tuoni, Energy analysis of ventilated and microventilated roofs, Sol. Energy 79 (2) (2005) 183–192, https://doi.org/10.1016/j.solener.2004.08.014.

[18] H. Wang, J. Wei, C. Guo, L. Yang, Z. Wang, Numerical investigation of the effects of different influencing factors on thermal performance of naturally ventilated roof, Energy 289 (2024), https://doi.org/10.1016/j.energy.2023.130039.

[19] A. Gagliano, F. Patania, F. Nocera, A. Ferlito, A. Galesi, Thermal performance of ventilated roofs during summer period, Energ. Buildings 49 (2012) 611–618, https://doi.org/10.1016/j.enbuild.2012.03.007.

[20] W. Athmani, L. Sriti, M. Dabaieh, Z. Younsi, The potential of using passive cooling roof techniques to improve thermal performance and energy efficiency of residential buildings in hot arid regions, Buildings, 13 (1) (2022) 21, https://doi.org/10.3390/buildings13010021.

[21] J. Yu, C. Qian, Q. Yang, T. Xu, J. Zhao, X. Xu, The energy saving potential of a new ventilation roof with stabilized phase change material in hot summer region, Renew. Energy 212 (2023) 111–127, https://doi.org/10.1016/J.RENENE.2023.05.012.

[22] A. Dimoudi, A. Androutsopoulos, S. Lykoudis, Summer performance of a ventilated roof component, Energ. Buildings 38 (6) (2006) 610–617, https://doi.org/10.1016/j.enbuild.2005.09.006.

[23] S. Lee, S.H. Park, M.S. Yeo, K.W. Kim, An experimental study on airflow in the cavity of a ventilated roof, Build. Environ. 44 (7) (2009) 1431–1439, https://doi.org/10.1016/j.buildenv.2008.09.009.

[24] C. Ferrari, A. Muscio, Ventilated pitched roof with forced ventilation and flow homogenizer device: testing and performance assessment, J. Phys. Conf. Ser. 1224 (1) (2019) 012027, https://doi.org/10.1088/1742-6596/1224/1/012027.

[25] C.J. Esparza-lópez, C. Escobar- Pozo, K.M. Al-obaidi, M.E. González-trevizo, Improving the thermal performance of indirect evaporative cooling by using a wet fabric device on a concrete roof in hot and humid climates, Energies 15 (6) (2022) 2213, https://doi.org/10.3390/en15062213.

[26] U. Berardi, P. La Roche, J.M. Almodovar, Water-to-air-heat exchanger and indirect evaporative cooling in buildings with green roofs, Energ. Buildings 151 (2017) 406–417, https://doi.org/10.1016/j.enbuild.2017.06.065.

[27] E. González Cruz, E. Krüger, Evaluating the potential of an indirect evaporative passive cooling system for Brazilian dwellings, Build. Environ. 87 (2015) 265–273, https://doi.org/10.1016/j.buildenv.2015.01.020.

[28] E. Krüger, L. Fernandes, S. Lange, Thermal performance of different configurations of a roof pond-based system for subtropical conditions, Build. Environ. 107 (2016) 90–98, https://doi.org/10.1016/j.buildenv.2016.07.021.

[29] L. Zhang, R. Zhang, Y. Zhang, T. Hong, Q. Meng, Y. Feng, The impact of evaporation from porous tile on roof thermal performance: A case study of Guangzhou's climatic conditions, Energ. Buildings 136 (2017) 161–172, https://doi.org/10.1016/j.enbuild.2016.12.012.

[30] S.M.S. Shokri Kuehni, E. Bou-Zeid, C. Webb, N. Shokri, Roof cooling by direct evaporation from a porous layer, Energ. Buildings 127 (2016) 521–528, https://doi.org/10.1016/J.ENBUILD.2016.06.019.

[31] S. Pedrazzi, G. Allesina, A. Muscio, Indirect evaporative cooling by sub-roof forced ventilation to counter extreme heat events, Energ. Buildings 229 (2020), https://doi.org/10.1016/j.enbuild.2020.110491.

[32] Ministero dell'Istruzione, "Linee guida Scuola Futura," 2022. [Online]. Available: https://pnrr.istruzione.it/wp-content/uploads/2022/05/LineeGuida_ScuolaFutura.pdf.

[33] G. Torriani, G. Lamberti, F. Fantozzi, F. Babich, Exploring the impact of perceived control on thermal comfort and indoor air quality perception in schools, J. Build. Eng. 63 (2023) 105419, https://doi.org/10.1016/J.JOBE.2022.105419.

[34] Ente Nazionale Italiano di Unificazione (UNI), "UNI 9460:2023 - Coperture discontinue - Istruzioni per la progettazione, l'esecuzione e la manutenzione di coperture realizzate con tegole di laterizio o calcestruzzo," 2023, *UNI*.
[35] International Organization for Standardization, "ISO 8996:2021 - Ergonomics of the thermal environment - Determination of metabolic rate," 2021, *International Organization for Standardization*.
[36] F. Ascione, L. Bellia, C. Mele, F. Minichiello, Air conditioning systems for school buildings: A case study, Proc Inst Civil Eng: Energy 169 (2) (2016) 52–78, https://doi.org/10.1680/jener.15.00007.
[37] H.G. Weller, G. Tabor, H. Jasak, C. Fureby, A tensorial approach to computational continuum mechanics using object-oriented techniques, Comput. Phys. 12 (6) (1998) 620–631, https://doi.org/10.1063/1.168744.
[38] European Committee for Standardization (CEN), "EN ISO 6946:2017 – Building components and building elements – Thermal resistance and thermal transmittance – Calculation methods," 2017, *CEN*.
[39] L. Susanti, H. Homma, H. Matsumoto, Y. Suzuki, M. Shimizu, Numerical simulation of natural ventilation of a factory roof cavity, Energ. Build. 42 (8) (2010) 1337–1343, https://doi.org/10.1016/j.enbuild.2010.03.002.